JCI insight

SARS-CoV-2-associated ssRNAs activate inflammation and immunity via TLR7/8

Valentina Salvi, … , Silvano Sozzani, Daniela Bosisio

JCI Insight. 2021. https://doi.org/10.1172/jci.insight.150542.

Research In-Press Preview Immunology

Graphical abstract

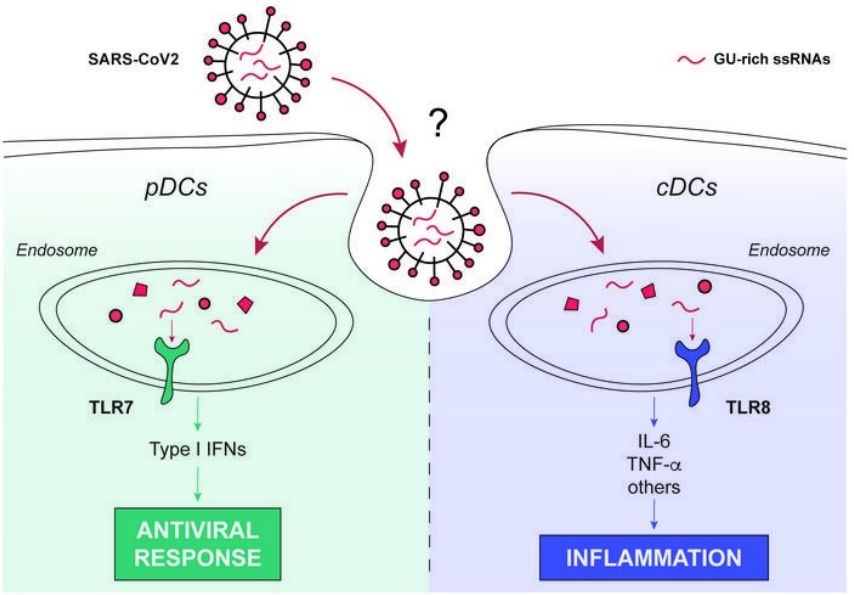

SARS-CoV-2-associated ssRNAs activate inflammation and immunity via TLR7/8

Valentina Salvi[1], Hoang Oanh Nguyen[1], Francesca Sozio[1,2], Tiziana Schioppa[1,2], Carolina Gaudenzi[1], Mattia Laffranchi[1], Patrizia Scapini[3], Mauro Passari[1], Ilaria Barbazza[1], Laura Tiberio[1], Nicola Tamassia[3], Cecilia Garlanda[2,4], Annalisa Del Prete[1,2], Marco A. Cassatella[3], Alberto Mantovani[2,4,5,*], Silvano Sozzani[6,7]* and Daniela Bosisio [1,*]

[1] Department of Molecular and Translational Medicine, University of Brescia, Italy

[2] IRCCS Humanitas Research Hospital, Rozzano (MI), Italy.

[3] Department of Medicine, Section of General Pathology, University of Verona, Italy

[4] Department of Biomedical Sciences, Humanitas University, Pieve Emanuele (MI), Italy.

[5] The William Harvey Research Institute, Queen Mary University of London, London, UK.

[6] Laboratory Affiliated to Istituto Pasteur Italia-Fondazione Cenci Bolognetti, Department of Molecular Medicine, Sapienza University of Rome, Rome, Italy

[7] IRCCS Neuromed, 86077, Pozzilli (IS), Italy

* Correspondence:

Daniela Bosisio, University of Brescia, Viale Europa 11, 25123 Brescia; Tel. +39-030-3717700; daniela.bosisio@unibs.it

Silvano Sozzani, Sapienza University of Rome, Viale Regina Elena 291, 00161 Roma; Tel. +39-06-49255115; silvano.sozzani@uniroma1.it

Alberto Mantovani, Humanitas University, Via Rita Levi Montalcini 4, 20090 Pieve Emanuele Milano; Tel. +39-02-82242444,45,46; alberto.mantovani@humanitasresearch.it

Running title: SARS-CoV-2-specific PAMPs activate TLR7 and TLR8

Abstract

The inflammatory and IFN pathways of innate immunity play a key role in both resistance and pathogenesis of Coronavirus Disease 2019 (COVID-19). Innate sensors and SARS-CoV-2-Associated Molecular Patterns (SAMPs) remain to be completely defined. Here we identify single-stranded RNA (ssRNA) fragments from SARS-CoV-2 genome as direct activators of endosomal TLR7/8 and MyD88 pathway. The same sequences induced human DC activation in terms of phenotype and functions, such as IFN and cytokine production and Th1 polarization. A bioinformatic scan of the viral genome identified several hundreds of fragments potentially activating TLR7/8, suggesting that products of virus endosomal processing potently activate the IFN and inflammatory responses downstream these receptors. In vivo, SAMPs induced MyD88-dependent lung inflammation characterized by accumulation of proinflammatory and cytotoxic mediators and immune cell infiltration, as well as splenic DC phenotypical maturation. These results identify TLR7/8 as crucial cellular sensors of ssRNAs encoded by SARS-CoV-2 involved in host resistance and disease pathogenesis of COVID-19.

Keywords: Pattern Recognition Receptors, Pathogen Associated Molecular Patterns, cytokine storm, Type I IFN, dendritic cells.

Introduction

SARS coronavirus 2 (SARS-CoV-2), is a positive-sense ssRNA virus belonging to the family of Coronaviridae, also including the closely related Middle East respiratory syndrome coronavirus (MERS-CoV) and SARS-CoV (1). In a subgroup of patients, SARS-CoV-2 infection (Coronavirus disease 2019, COVID-19) develops as acute respiratory distress syndrome featuring intense lung injury, sepsis-like manifestations and multi-organ failure (2) associated with overt production of pro-inflammatory cytokines that directly correlates with poor prognosis (3). This clinical condition suggests that an overactive innate immune response may unleash virus-dependent immune pathology (4). Innate immune activation is also responsible for inducing the protective antiviral state, largely mediated by the release of type I IFNs. Indeed, inborn errors in type I IFN production and amplification (5) or pre-existing blocking auto-antibodies against members of the IFN family of cytokines (6) were found to correlate with unfavorable prognosis.

DCs act as crucial messengers linking innate and adaptative immunity against viral infections (7, 8). Within DC heterogeneity, plasmacytoid DCs (pDCs) play an important role as the major source of type I IFN in response to viral infection, while conventional DCs (cDCs) respond to a vast variety of pathogens by producing pro-inflammatory cytokines and are the main responsible for T cell activation (9–11). pDCs sense ssRNA viruses through TLR7 (12), an endosomal receptor activated by genomic fragments rich in guanine (G) and uracil (U), derived by endosomal processing of the virus independently of infection (13). By contrast, cDCs express the closely related TLR8 (14). Despite the fact that TLR7 and TLR8 display high structural and functional homology, similar ligand specificity (15) and recruit the same signaling intracellular adaptor molecule, MyD88 (16), the signaling pathways of these two TLRs diverge in the functional significance, with TLR7 more involved in the antiviral immune response and TLR8 mastering the production of pro-inflammatory cytokines. Both cDCs and pDCs were shown to be reduced in the blood of severe acute COVID-19 patients (17, 18) as a possible result of cell activation (19), but the mechanisms of SARS-CoV-2 recognition and activation

by innate immune cells still need to be identified. This study characterizes the first SARS-CoV-2-associated molecular patterns (SAMPs) and identifies the TLR7/8/MyD88 axis as a crucial pathway in the activation of human pDCs and cDCs.

Results

Identification of potential ssRNA SAMPs

Based on previous work identifying RNA40, a ssRNA rich in guanine and uracil (GU-rich) from the U5 region of HIV-1, as the first natural agonist of TLR7 and TLR8 (20) and on known features of TLR7/8 ligands (15, 21, 22), we searched for putative immunostimulatory sequences within the SARS-CoV-2 ssRNA genome. Our bioinformatic scan revealed 491 GU-rich sequences, among which more than 250 also bearing at least one "UGUGU" Interferon Induction Motif (IIM) (15, 20, 21) (Suppl. Table 1).

We hypothesized that these sequences may represent so far unidentified SAMPs responsible for viral recognition and immune activation via endosomal TLR triggering. The elevated number of sequences detected suggests that, upon endosomal engulfment, the fragmentation of the SARS-CoV-2 genome may generate many TLR7/8-triggering sequences, thus displaying high chances to contact and activate the IFN and inflammatory responses downstream these receptors.

To validate the stimulatory potential on innate immune cells, two representative sequences, SCV2-RNA1 and SCV2-RNA2, were chosen within the previous list, synthesized and tested in *in vitro* and *in vivo* models of inflammation.

ssRNA SAMPs activate human monocyte-derived DCs (moDCs)

moDCs, a model of inflammatory cDCs expressing a wide variety of TLRs (7, 23–25), were treated with increasing concentrations of SCV2-RNA1 and SCV2-RNA2 along with HIV-1-derived RNA40 (20), used as a positive control. U/A alternated control sequences SCV2-RNA1A and SCV2-RNA2A were used as negative controls (see materials and methods). Figure 1A shows that both fragments efficiently activated cytokine secretion by moDCs. In particular, we observed potent induction of pro-inflammatory cytokines (TNF-α, IL-6), of the Th1-polarizing cytokine IL-12 and chemokines recruiting

polymorphonuclear neutrophils (CXCL8), myelomonocytic cells (CCL3) and Th1- and cytotoxic effectors cells (CXCL9). Especially at low concentrations, SCV2-RNA1 and SCV2-RNA2 were more efficient than HIV-1-derived RNA40. In all experimental conditions, U/A alternated SCV2-RNA1A and SCV2-RNA2A did not induce cytokine secretion. SCV2-RNA1 and SCV2-RNA2 also induced moDC phenotypical maturation in terms of CD83, CD86 and CCR7 expression (Figure 1B). Similarly to cytokine secretion, upregulation of maturation markers by RNA40 was less effective. These results demonstrated that both SCV2-RNA1 and SCV2-RNA2 behave as SAMPs endowed with potent DC stimulatory capacity. Because of their similar potency, further experiments were carried out using a mixture of the two SAMPs (indicated as SCV2-RNA), a condition that may also better mimic a physiological stimulation by multiple sequences derived from SARS-CoV-2 genome endosomal fragmentation.

ssRNA SAMPs activate T cell responses

The impact of SAMPs on the ability of DCs to stimulate T cell functions was investigated in co-culture experiments of SAMP-activated DCs with allogeneic naïve $CD4^+$ and $CD8^+$ T cells. Figure 2A shows that SAMP-activated DCs induced proliferation of both naïve $CD4^+$ (left) and $CD8^+$ (right) T cells. Activated $CD4^+$ T cells produced IFN-γ but no IL-4, a typical Th1-effector phenotype (Figure 2B). Functional activation of $CD8^+$ T cells was similarly demonstrated by the detection of secreted IFN-γ (Figure 2C, left panel) and the intracellular accumulation of Granzyme B (GrB, right panel), a marker of a cytotoxic phenotype. None of these effects were observed when DCs were activated with U/A alternated SAMPs.

These experiments demonstrated that phenotypical DC maturation induced by SAMPs (Figure 1B) is paralleled by the acquisition of T-cell activating capabilities. Thus, SAMPs have the ability to induce a Th1-oriented immune response.

ssRNA SAMPs activate human primary DCs

The ability of SCV2-RNAs to activate DCs was further investigated using primary circulating cDCs (comprising $CD141^+$ cDC1 and $CD1c^+$ cDC2) and $BDCA2^+$ pDCs. SCV2-RNA efficiently induced the secretion of TNF-α and IL-6 (Figure 3A) and the expression of maturation markers, such as CD86 and CCR7 (Figure 3B) in cDCs. Similarly, SAMPs stimulated the release of IFN-α and TNF-α by pDCs (Figure 3C), as well as their maturation in terms of CD86 upregulation and BDCA2 reduction (Figure 3D). Similarly to previous results, U/A alternated control sequences did not activate cytokine production or maturation in either pDCs and cDCs (not shown).

ssRNA SAMPs activate the TLR8/MyD88/NF-κB axis in moDCs

The cellular sensors responsible for SARS-CoV-2 detection by immune cells remain ill defined. To formally demonstrate the ability of SAMPs to functionally activate TLRs, experiments were performed in HEK293 cells stably transfected with human TLR7 and TLR8 together with a NF-κB reporter gene. Figure 4A depicts the SAMP-dependent activation of NF-κB and luciferase production in both TLR7- and TLR8-expressing cells. NF-κB activation was also detected in SCV2-RNA-stimulated moDCs (Figure 4B). Since both TLR7 and TLR8 signal through the common adaptor MyD88, siRNA interference was performed in moDCs. Figure 4C (left panel) shows that MyD88-specific siRNA could decrease by about 50% the levels of MyD88 mRNA, while the expression of the TLR3-related adaptor TRIF and RLR-related MAVS was not affected. Consistent with this result, IL-6 production by SCV2-RNA was also decreased, supporting a role for MyD88 in moDC activation by SCV2-RNA (Figure 4C, right panel). Because SAMPs, despite designed to activate TLR7/8, may also engage other PRRs expressed by moDCs, we also performed TRIF and MAVS siRNA interference. While siRNAs efficiently and specifically inhibited the expression of target genes (Figure 4C, left panel), they failed to reduce IL-6 production by SCV2-RNA (Figure 4C, right panel). The predominant role of the MyD88/NF-κB

pathway as compared with that of TRIF/MAVS/IRF-3 was also supported by the lack of SCV2-RNA-dependent induction of nuclear translocation of IRF-3, a transcription factor downstream TLR3 and RLRs (not shown).

moDCs are known to respond mainly to TLR8 ligands and to express negligible levels of TLR7 mRNA (14, 23). mRNA and protein expression analysis of TLR7 and TLR8 confirmed selective expression of TLR8 in our experimental setting (Suppl. Figure 1A and B). Based on this, we performed TLR8 siRNA in moDCs, showing a reduction in SCV2-RNA-dependent activation correlating to the levels of mRNA reduction (Figure 4D).

Next, moDCs were stimulated in the presence of CU-CPT9a, a specific TLR8 inhibitor (26). CU-CPT9a inhibited both NF-κB nuclear translocation (Figure 4E) and IL-6 production when cells were stimulated with SCV2-RNA or R848 (TLR7/8 ligand) (Figure 4F). On the other hand, the TLR8 inhibitor did not affect the stimulation by LPS, a TLR4 ligand (Figure 4E and F). Finally, we found that SCV2-RNA colocalizes with TLR8 within moDCs (Suppl. Figure 1C).

ssRNA SAMPs act as TLR7/8 ligands in primary DCs

TLR7 and TLR8 display a mutual exclusive expression in primary DCs. Indeed, cDCs express TLR8 as their unique endosomal ssRNA receptor, while pDCs express TLR7 (14). Consistent with this, CU-CPT9a blocked the production of pro-inflammatory cytokines in cDCs (Figure 5A), but not in TLR7-expressing pDCs (Figure 5B). Our effort to block TLR7 signaling using commercially available receptor antagonists was unsuccessful since none of these inhibitors blocked TLR7 activation in pDCs stimulated with R848 or Imiquimod (data not shown). As an alternative strategy to demonstrate the involvement of TLR7 in SCV2-RNA sensing we performed TLR desensitization (21). pDCs were stimulated with

SCV2-RNA or R848 or left untreated, washed, and then re-stimulated with R848. Figure 5C shows that, upon re-stimulation, only untreated cells could respond to R848 in terms of IFN-α and TNF-α production as a result of TLR7 desensitization by its ligand R848 as well as by SCV2-RNA. The limited yield following blood DC purification hampered the use of siRNAs. However, the involvement of endosomal TLRs as SCV2-RNA receptors was further supported by the blocking of cytokine release in both cDCs (Figure 5D) and pDCs (Figure 5E) by chloroquine (CQ), a drug known to block endosomal TLR triggering by interfering with endosomal acidification (27).

ssRNA SAMPs induce DC activation and lung inflammation in vivo

To address the capacity of SAMPs to induce inflammation and immune activation *in vivo*, we first investigated if SAMPs can also trigger murine TLR7, the only GU-rich ssRNA-sensing TLR in mouse (20). Murine TLR7 activation by SAMPs could be hypothesized based on previous works demonstrating that activation of human TLR7/8 and murine TLR7 by common GU-rich ssRNA ligands (20, 28). In support of this, we show that TLR7-expressing RAW264.7 cells (Figure 6A) responded to SAMP stimulation by producing TNF-α, an effect that was reduced by CQ pretreatment (Figure 6B) confirming that SCV2-RNA activate murine cells, presumably via TLR7. In addition, splenocytes from MyD88$^{-/-}$ mice did not respond to SCV2-RNA stimulation either in terms of pro-inflammatory cytokine production (Figure 6D) and of TLR modulation (Suppl. Figure 2) despite expressing similar levels of TLRs as compared to WT mice (Figure 6C).

Based on these results, C57Bl6/J WT and MyD88$^{-/-}$ mice were injected i.v. with SAMPs or vehicle and sacrificed 6 hours later. A significant increase of type I IFN was detected in the sera of WT SAMP-treated mice indicating systemic immune activation (Figure 6E). Consistent with this, SAMPs

188 induced the upregulation of CD40 and CD86 on splenic pDCs ($CD11c^{int}MHC\text{-}II^{+}B220^{+}SiglecH^{+}$)
189 (Figure 6F). Activation of splenic cDC1s ($CD11c^{+}MHC\text{-}II^{+}CD8\alpha^{+}CD11b^{-}$) and cDC2s ($CD11c^{+}MHC\text{-}II^{+}$
190 $CD8\alpha^{-}CD11b^{+}$) was also detected (Figure 6G and H). Figure 7A shows that SAMP treatment induced
191 the expression of pro-inflammatory cytokines TNF-α, IL-1β, IL-6 and of IFN-α and IFN-γ in the lung.
192 In addition, a marked increase in the expression of chemokines active on myeloid and Th1 effector
193 cells (i.e. CCL3, CCL4 and CXCL10) was also detected. Conversely, CCL20 and CCL22, two
194 chemokines active in Th17 and Th2 T cell recruitment, were not increased (Figure 7B). We could also
195 detect the accumulation of molecules involved in cytotoxic tissue damage such as GrB and TRAIL
196 (Figure 7C) that, given the short kinetics of stimulation, may reflect the recruitment of NK cells to the
197 lungs. The increase of CD45 and MHC-II levels (data not shown) further suggested immune cell
198 infiltration, which was confirmed by histological analysis. Lung histology revealed a marked
199 infiltration of inflammatory cells into peri-bronchial and peri-vascular connective tissue and alveolar
200 septal thickening in SAMP-treated mice (Figure 7D). On the contrary, SAMP administration to
201 $MyD88^{-/-}$ mice did not induce any inflammatory response, including the increase of circulating levels
202 of type I IFN, DC maturation and the generation of a lung infiltrate (Fig. 6 D-H and Figure 7). These
203 data extend to the *in vivo* condition the observation that SAMPs use a TLR/MyD88-dependent
204 pathway to trigger a type I IFN/pro-inflammatory activation program and highlight lung as a
205 primary target organ.
206

Discussion

Here, we report that two short sequences within the ssRNA genome of SARS-CoV-2 activate the production of type I IFNs and the T cell-activating ability of human DCs by triggering endosomal TLR7 and TLR8. Of note, these sequences represent prototypical examples of the several hundreds of potential TLR ligands identified by SARS-CoV-2 genome scan. This finding is in line with previous work demonstrating a twenty-fold higher density of GU-rich fragments in the closely related SARS-CoV as compared to HIV-1 (29) and with a recent bioinformatic study showing that SARS-CoV-2 encodes a number of such fragments even larger than SARS-CoV (30). Thus, endosomal processing of SARS-CoV-2 nucleic acids may give rise to multiple fragments endowed with the property to trigger innate immune activation.

TLR7/8 are sensors of ssRNA viruses including coronaviruses. In the past, TLR7-dependent recognition of MERS-CoV and human and murine pDC activation was demonstrated (31). In addition, murine coronavirus activated protective type-I IFN production by TLR7-expressing murine pDC (32) and ssRNA SARS-CoV genome was shown to induce TLR7/8 dependent cytokine secretion by human PBMCs and RAW264.7 murine cells (29). By contrast, the involvement of TLR7/8 in the immune response against SARS-CoV-2, as well as their role in COVID-19 pathogenesis and therapeutic potential has been only hypothesized (33). Notably, very rare loss-of-function variants of TLR7 in two independent families were associated with severe COVID-19 in males (34). Thus, our report on the ability of SAMPs to activate the TLR7/8 and MyD88 pathways provides the missing link between clinical evidence and molecular knowledge on the cellular sensors for SARS-CoV-2 detection. Viral recognition by endosomal TLRs takes place before and independently of infection, as a consequence of pathogen endocytosis (13). Indeed, pDCs were reported to be resistant to infection, although they were activated by SARS-CoV-2 (35). This is an important process that gives innate immune cells the

opportunity to activate early antiviral response. One limitation of our experimental approach is that it does not shed light on the actual triggering of endosomal TLRs during active SARS-CoV-2 infection. However, this is a likely event based on the reported SARS-CoV-2-dependent pDC activation, which use TLR7 as the main ssRNA receptor (12, 35). In addition, endosomal TLRs expressed by innate immune cells were shown to be activated by viral RNAs packaged within extracellular vesicles by infected tissue cells (36), a mechanisms that is mimicked by SCV2-RNA-delivery by liposomal particles. Indeed, in another experimental setting, liposome-delivered ssRNA40 from HIV-1 activated human macrophages via TLR8 in a way that recapitulated intact HIV-1 administration (37). It remains to be elucidated if SARS-CoV-2 uptake for endosomal processing is a direct process or mediated by receptors, such as ACE2 or CD147 (38).

DCs are heterogeneous cells that master activation of inflammation and antiviral responses, adaptive immune responses and tolerance as well (7, 8). These functions are largely shared among different phenotypical and functional DC subsets (39). Indeed, pDCs are the major producers of type I IFNs in response to viral infections (10–12), while cDCs, and cDC2s in particular, sustain inflammation via cytokine secretion and activate naïve T cells (39). Notably, this specialization mirrors the respective expression and function of TLR7 and TLR8 (14). The protective role of TLR7 and type I IFNs in life-threatening COVID-19 has been documented based on the clinical outcome of patients with inborn errors in type I IFN immunity, producing blocking auto-Abs against different types of type I IFNs (5, 6) or expressing loss-of-function variants of TLR7 (34). Therefore, SAMPs may represent one of the essential signals in the activation of an IFN response and Th1-oriented adaptive immunity (40, 41). In this regards it is of note that SARS-CoV-2 infection affected the number of pDCs in vivo (17, 18) and primary virus isolates induced the activation of pDCs, *in vitro* (35). By contrast, an aggravated inflammatory response causes damage to the host and frequently advances to ARDS in severe COVID-19 patients. Here, we show that the activation program induced by SAMPs is not

254 restricted to type I IFNs, but encompassed the production of pro-inflammatory cytokines and the
255 generation of Th1-oriented responses, which may contribute to the exuberant pro-inflammatory
256 response observed in life-threatening COVID-19 (42). Whether TLR8 or cDC overactivation or genetic
257 variants are involved in this process is difficult to speculate, and more studies on selected patient
258 cohorts are needed. However, TLR7 and TLR8 selective agonists or antagonists, inducing antiviral
259 interferon response and/or controlling inflammation, deserve consideration and have entered Phase
260 II clinical trial as interesting therapeutic options to control the different manifestations of COVID-19
261 (https://clinicaltrials.gov/ct2/show/NCT04448756). ssRNA-sensing TLRs are expressed also by cells
262 other than DCs such as macrophages, as well as by peripheral tissues such as lung, bronchus, rectum,
263 and cerebral cortex (38). Thus, other cells may contribute to the complex balance of protective versus
264 detrimental immune activation (4). Finally, since the magnitude of TLR activation differs in
265 individuals, such as elderly people, differences in TLR activation may help explain differences in the
266 quality of the antiviral immune response independently of SAMP potency (39).

267 By all means, other SAMPs and DAMPs as well as the simultaneous engagement of different
268 PRRs are likely to contribute to COVID-19-associated protective response and cytokine storm,
269 including cytosolic sensors, such as retinoid-inducible gene-I (RIG-I)-like receptors (43), Interferon
270 Induced proteins with tetratricopeptide repeats, or members of a large group of RNA-binding
271 molecules with poorly defined ligand specificity (43). A search for specific candidate ligands of cytosolic
272 RNA-sensors was hampered because the scarce definition of their ligand consensus sequences.
273 However, the finding that SARS-CoV-2 can evade innate immune restriction provided by intracellular
274 RNA-sensors via methylation the 5'-end of its cellular mRNAs (44) further reinforces the role for TLRs
275 as crucial sentinels and regulators of immune response to SARS-CoV-2 infection. SARS-CoV-2 is known
276 to induce inflammasome assembly despite the exact mechanism still need to be characterized (45, 46).
277 Since intracellular nucleic acid sensors are known to activate inflammasomes (47), and TLR activation
278 is intimately connected with inflammasome functions (48, 49), it is possible that SCV2-RNAs used in
279 this study may also contribute to activate this pathway.

In conclusion, this work describes that SARS-CoV-2 is as a potential powerful source of immunostimulatory nucleic acid fragments and identifies the first SARS-CoV-2-specific PAMPs endowed with the ability to promote inflammation and immunity triggering TLR7 and TLR8. Based on previous works demonstrating a) the crucial protective role of type I IFNs against COVID-19 (5, 6); b) the crucial protective role of TLR7 against life-threatening SARS-CoV-2 infection (34) and c) pDC activation *in vitro* by SARS-CoV-2 (35), we believe that our findings fill a gap in the understanding of SARS-CoV-2 host-pathogen interaction.

Methods

Identification of potential TLR7/8-triggering ssRNA PAMPs

The reference SARS-CoV-2 genome (NC_045512, positive strand) was scanned for GU-rich ssRNA fragments with the SequenceSearcher tool in the Fuzzy mode (50). We defined "GU-enriched sequences" short strings with a maximal length of 20 bp, that were composed for more than 40% of the length by "GU" and/or "UG" pairs. The identified 491 GU-rich sequences were further selected based on the content of at least one "UGUGU" Interferon Induction Motif (IIM)(21) (see Suppl. Table 1). Within this list, the following were selected based on the particular enrichment in IIM (21) and synthesized by Integrated DNA Technologies (IDT) for subsequent studies: SCV2-RNA1 5′-UGCUGUUGUGUGUU*U-3′ (genome position: 15692-15706); SCV2-RNA2 5′-GUGUGUGUGUUCUGUUAUU*G-3′ (genome position: 20456-20475). These sequences were checked for uniqueness with BLAST in the database RefSeq Genome Database (refseq_genomes) within the RNA viruses (taxid: 2559587). Two additional sequences were synthesized, in which "U" was substituted with "A", in order to impair TRL7/8 stimulation (SCV2-RNA1A and SCV2-RNA2A) (15, 20). * indicates a phosphorothioate linkage.

Cell preparation and culture

Peripheral blood mononuclear cells (PBMC) were obtained by density gradient centrifugation and monocytes were subsequently purified by immunomagnetic separation using anti CD14-conjugated magnetic microbeads (Miltenyi Biotec) according to the manufacture's protocol and as previously published (23). Briefly, monocytes were cultured for 6 days in tissue culture plates in complete medium (RPMI 1640 supplemented with 10% heat-inactivated, endotoxin free FBS, 2 mM L-Glutamine, penicillin and streptomycin (all from Gibco, Thermo Fisher Scientific) in the presence of 50 ng/ml GM-CSF and 20 ng/ml IL-4 (Miltenyi Biotec). Untouched peripheral blood cDC1 and cDC2

(cDCs) and pDCs were obtained from PBMC after negative immunomagnetic separation with the Myeloid Dendritic Cell Isolation kit (Miltenyi Biotec) and the Plasmacytoid Dendritic Cell Isolation kit II (Miltenyi Biotec), respectively. pDCs were cultured in completed RPMI medium with 20 ng/ml IL-3 (Miltenyi Biotec). RAW264.7 cells were purchased from American Type Culture Collection (ATCC) and cultured in DMEM complemented with 10% FBS.

Cell stimulation

Complexation of RNA with DOTAP Liposomal Transfection Reagent (Roche) was performed as previously described (21). Briefly, 5 μg RNA (either SCV2-RNA1 alone, SCV2-RNA2 alone or 2.5 μg SCV2-RNA1+ 2.5 μg SCV2-RNA2 to obtain SCV2-RNA) in 50 μl HBS buffer (20 mM HEPES, 150 mM NaCl, pH 7.4) was combined with 100 μl DOTAP solution (30 μl DOTAP plus 70 μl HBS buffer) and incubated for 15 minutes at RT. Where indicated, cells were pretreated for 1 hour with Chloroquine or CU-CPT9a or stimulated with the following TLR agonists: LPS (100 ng/ml) and R848 (1 μg/ml) (all from Invivogen).

siRNA silencing in moDCs

Differentiating monocytes at day 2 of culture were transfected with MyD88 or TRIF or MAVS or TLR8 Silencer Select Validated siRNA or with a control siRNA (all at 50 nM final concentration; Ambion, Thermo Fisher Scientific) using Opti-MEM I reduced serum medium and Lipofectamine RNAiMAX transfection reagent (Thermo Fisher Scientific) as previously described (51). Transfected cells were incubated for 72 hours and then stimulated for 24 hours with SCV2-RNA. The effects of mRNA

silencing by siRNA was investigated by qPCR (quantitative PCR) using specific QuantiTect primer Assay (Qiagen).

Cytokine detection

TNF-α, IL-6, IL-12p70, CXCL8, CXCL9, CCL3 and mouse TNF-α were measured by ELISA assay (R&D Systems). Human IFN-α was detected using specific Module Set ELISA kit (eBioscience). Mouse IFN-α was measured by a bioluminescence kit (InvivoGen). All assays were performed on cell free supernatants according to the manufacturer's protocol.

Flow cytometry

Human and mouse DCs were stained with the following antibodies from Miltenyi Biotec or as specified: Vioblue-conjugated anti-human CD86 (clone FM95), PE-conjugated anti-human CD83 (clone REA714), FITC-conjugated anti-human BDCA2 (clone AC144), APC-conjugated anti-human CCR7 (clone REA546), VioGreen-conjugated anti-mouse CD45 (clone REA737), VioBlue or FITC-conjugated anti-mouse MHC-II (clone REA564), PerCP-Vio 700-conjugated anti-mouse CD11c (clone REA754), PE-conjugated anti-mouse SiglecH (clone 551.3D3), PE-Vio 615-conjugated anti-mouse CD11b (clone REA592), VioBlue-conjugated anti-mouse CD8a (cloneREA601), PE-Vio 770-conjugated anti-mouse B220 (clone RA3-6B2), APC-conjugated anti-mouse CD3 (clone REA641), APC-conjugated anti-mouse CD19 (clone REA749), APC-conjugated anti-mouse CD49b (clone DX5), APC-conjugated anti-mouse Ly6G (clone REA526), PE-conjugated anti-mouse CD40 (clone REA965), FITC-conjugated anti-mouse CD40 (clone HM40-3, Biolegend) and APC-CY7-conjugated anti-mouse CD86 (clone GL-1, Biolegend). Samples were read on a MACSQuant Analyzer (Miltenyi Biotec) and

355 analysed with FlowJo (Tree Star Inc.). For intracellular detection of Granzyme B, cells were fixed and
356 permeabilized using the Inside Stain kit (Miltenyi Biotec) and stained with APC-conjugated anti-
357 Granzyme B (clone REA226, Miltenyi Biotec). Cell viability was assessed by LIVE/DEAD staining
358 according to the manufacturer's instruction (Molecular Probes, Thermo Fisher Scientific). The gating
359 strategy of mouse DCs was as follow: cells were first defined from FSC-A/SSC-A, over doublet
360 exclusion and gating on Live, $CD45^+$ LIN^- cells (defined as CD3/CD19/CD49b/$Ly6G^-$). Therefore,
361 pDCs were identified as $CD11c^{int}$MHC-$II^+B220^+SiglecH^+$ cells; cDC1s as $CD11c^+$MHC-$II^+CD8\alpha^+$CD11b;
362 cDC2s as $CD11c^+$ MHC-II^+ $CD8\alpha^-CD11b^+$ (52).
363
364 **NF-κB luciferase reporter assay**
365 TLR-specific activation assays were performed using human HEK293 cells (ATCC) expressing
366 luciferase under control of the NF-κB promoter and stably transfected with human TLR7 and TLR8
367 as previously described (21). Briefly, 25000 cells were seeded in complete DMEM without antibiotics
368 in 96-well plates for 24 hours and then stimulated with 10 μg/ml SCV2-RNA for additional 24 hours.
369 After stimulation, cells were lysed using ONE-Glo EX Luciferase Assay System (Promega) according
370 to the manufacturer's recommendations and assayed for luciferase activity using the
371 EnSightMultimode Plate Reader (PerkinElmer). HEK293 cells were maintained in DMEM
372 supplemented with 10% FBS and specific selection antibiotics were added.
373
374 **SDS-PAGE and Western Blot**
375 Following the indicated stimulations, moDCs were washed twice with PBS and lysed in L1 buffer (50
376 mM Tris-HCl, pH 8.0; 2 mM EDTA; 0.1% NP-40 and 10% glycerol) supplemented with inhibitors (1

mM Na_3OV_4, 2 mM DTT, 1 mM NaF, 1 mM PMSF, and protease inhibitor cocktail; all form MilliporeSigma) to separate cytoplasmic proteins. Nuclear pellets were washed twice with L1 buffer with inhibitors and then lysed in NP-40 Lysis buffer (50 mM Tris-HCl, pH 8.0; 250 mM NaCl; 1 mM EDTA; 0.1% NP-40; and 10% glycerol) with inhibitors. For the analysis of TLR expression, moDCs and HEK293-transfected cells were lysed in NP-40/Triton lysis buffer (10 mM Tris-HCl, pH 7.9; 150 mM NaCl; 0.6% NP-40; and 0.5% Triton X-100) supplemented with inhibitors. Equal amounts of extracts were analyzed through SDS-PAGE followed by Western blotting with antibodies against NF-kB p65 (rabbit polyclonal, C-20 cat. sc-372, Santa Cruz Biotechnology inc.), Lamin B (goat polyclonal, C-20 cat. 6216, Santa Cruz Biotechnology inc.), TLR7 (rabbit monoclonal, cat. 5632, Cell Signaling Technologies), TLR8 (rabbit monoclonal, cat. 11886, Cell Signaling Technologies) and β-actin (mouse monoclonal, C4, cat. sc-47778, Santa Cruz Biotechnology inc.). Protein bands were detected with SuperSignal West Pico Chemiluminescent Substrate (Pierce) and quantified by computerized image analysis using Image LabTM software (Bio-Rad). Data were normalized based on β-actin or Lamin B content.

Immunofluorescence

moDCs were incubated with Atto-488-tagged SCV2-RNA1 (synthesized by Bio-Fab research) for 15 minutes, fixed with 4% paraformaldehyde (Pierce) for 10 minutes and then seeded on glass slides by cytospin. After permeabilization with 100% cold methanol for 5 minutes, cells were labelled with a rabbit monoclonal anti-human TLR8 (cat. 11886, Cell Signaling Technologies). A conjugate Alexa Fluor 594 anti-rabbit (A-11072, Thermo Fisher Scientific) was used as a secondary antibody. Glass slides were mounted using Prolong antifade with DAPI (Thermo Fisher Scientific). Cells were

analyzed under a Zeiss Observer Z1 epifluorescence microscope equipped with a Plan-Apochromat 100x/ 1.4 numerical aperture oil objective and ApoTome2 imaging system for optical sectioning. Z-stack images were elaborated through AxioVision 3D and extended focus modules.

T cell proliferation assay

Experiments using T cells were conducted according to the "Minimal Information about T Cell Assays" (MIATA) guidelines. Allogenic naïve CD4+ T cells and CD8+ T cells were isolated from buffycoats using the naïve CD4+ T cell Isolation kit II (Miltenyi Biotec) and CD8+ T cell Isolation kit (Miltenyi Biotec), respectively. Purified T cells were counted by flow cytometry and labeled with CellTrace-CFSE (Molecular Probes, Thermo Fisher Scientific) at a final concentration of 5 μM. Subsequently, T cells (1x105 cells/well) were cocultured with graded numbers of allogeneic moDCs in 96-well round-bottom culture plates in complete RPMI medium. After 6 days, alloreactive T cell proliferation was assessed by measuring the loss of the dye CellTrace-CFSE upon cell division using flow cytometry. Positive controls of T cell proliferations were routinely performed using IL-2 plus PHA. Response definition criteria were defined post-hoc. Dead cells were excluded by LIVE/DEAD staining according to the manufacturer's instruction. These experiments were performed using general research investigative assays. Raw data can be provided per request.

Analysis of T cell cytokine production

After 6 days of coculture, helper T cells were restimulated with 200 nM PMA (Sigma-Aldrich) plus 1 μg/ml of ionomycin (Sigma) for 5 hours. Brefeldin A (5 μg/ml, Sigma) was added during the last 2 hours. For intracellular cytokine production, cells were fixed and permeabilized with Inside Stain kit

(Miltenyi Biotec) and stained with FITC-conjugated anti-IFN-γ (clone 45-15, Miltenyi Biotec) and PE-conjugated anti-IL-4 (clone 7A3-3, Miltenyi Biotec) following the manufacturer's recommendations. For $CD8^+$ T cells, after 6 days of coculture, IFN-γ production was assessed in the culture supernatants by ELISA (R&D system). Response definition criteria were defined post-hoc. These experiments were performed using general research investigative assays. Raw data can be provided per request.

***In vivo* experiments**

$MyD88^{-/-}$ mice (C57Bl6/J background) were kindly provided by S. Akira (Laboratory of Host Defense, Immunology Frontier Research Center (IFReC), Osaka University, Osaka, Japan). WT C57Bl6/J mice were purchased by Charles River Laboratories. All mice were housed in the specific pathogen-free animal facility of the Department of Medicine, University of Verona. Sex and aged-matched WT and $MyD88^{-/-}$ mice (8-10 week old) were anesthetized with isoflurane and injected i.v. in the retro-orbital vein with 300 µl DOTAP/SCV2-RNA mixture (20 µg/mouse) or with DOTAP alone. After 6 hours, mice were sacrificed and lungs, spleen and blood were harvested. Briefly, lungs were collected upon intracardiac perfusion with cold PBS. Left lung lobes were formalin fixed for 24 hours, dehydrated, and paraffin embedded for histological analysis. Right lungs were immediately frozen at -80°C and used for real-time PCR. Spleens were mechanically and enzymatically treated to obtain a single-cell suspension for cytofluorimetric and real-time PCR analysis.

Lung histological analysis

Histology was performed on three longitudinal serial sections (150 µm apart, 4 µm in thickness) from each left lung, stained with hematoxylin and eosin (H&E), and scanned by VS120 Dot Slide BX61

443 virtual slide microscope (Olympus Optical) as previously described (53).

444

445 **Quantitative PCR (qPCR)**

446 RNA was extracted using TRIzol reagent, treated with DNAse according to the manufacturer's
447 instructions and reverse transcription performed using random hexamers and MMLV RT (all from
448 Thermo Fisher Scientific). The SsoAdvanced Universal SYBR Green Supermix (Bio-Rad Laboratories)
449 was used according to the manufacturer's instructions. Reactions were run in triplicate on a StepOne
450 Plus Real-Time PCR System (Applied Biosystems) and analyzed by the StepOne Plus Software
451 (Version 2.3, Applied Biosystems). Sequences of gene-specific primers are listed in Suppl. Table 2.
452 Gene expression was normalized based on mouse RPL32 or human HPRT mRNA content.

453

454 **Statistical analysis**

455 Sample group normality was confirmed by Shapiro-Wilk test before application of parametric
456 statistical analysis. Statistical significance among the experimental groups was determined using
457 paired or unpaired Student's *t* test or one-way ANOVA with Dunnet's post-hoc test (GraphPad Prism
458 7, GraphPad Software) as indicated in each figure legend. $P < 0.05$ was considered significant; "n"
459 indicates the number of biological replicates and is specified in each figure legend.

460

461 **Study approval**

462 Buffy coats from blood donations of anonymous healthy donors were obtained and preserved by the
463 Centro Trasfusionale, Spedali Civili of Brescia according to the italian law concerning blood
464 component preparation and analysis. Procedures involving animal handling and care conformed to

protocols approved by the University of Verona in compliance with national (D.L. N.116, G.U., suppl. 40, 18-2-1992 and N. 26, G.U. March 4, 2014) and international law and policies (EEC Council Directive 2010/63/EU, OJ L 276/33, 22-09-2010; National Institutes of Health Guide for the Care and Use of Laboratory Animals, U.S. National Research Council, 2011). The study was approved by the Italian Ministry of Health (approval number 339/2015-PR). All efforts were made to minimize the number of animals used and their suffering.

Author Contributions: Conceptualization, D.B., M.A.C., A.M., S.S., V.S., A.D.P.; methodology, V.S., A.D.P., P.S., D.B., Ce.G.; software, M.L. and D.B.; validation and formal analysis, V.S., H.O.N. M.P., I.B.; investigation, V.S., H.O.N., F.S., T.S., M.L., P.S., L.T., I.B., M.P, N.T., Ce.G.; Ca.G.; data curation, V.S., H.O.N., F.S., M.L., I.B.; writing—original draft preparation, D.B., V.S., H.O.N.; writing—review and editing, A.M., S.S., M.A.C., P.S., A.D.P, D.B.; visualization, H.O.N. and I.B.; supervision, D.B., M.A.C., S.S.; funding acquisition, S.S., M.A.C, D.B., P.S. All authors have read and agreed to the published version of the manuscript.

Acknowledgements

This research was funded by the Italian Ministry of Health (Bando Ricerca COVID-2020-12371735 to S.S.), Italian Ministry of the University and Research (MUR-PRIN 20178ALPCM_005 to D.B. and MUR-PRIN 20177J4E75_004 to M.A.C.), Associazione Italiana per la Ricerca sul Cancro (AIRC IG-20339 to M.A.C. and IG-20776 to S.S.), University of Verona (RBVR17NCNC to P.S.) and University of Brescia (Fondi Locali 2019 and 2020 to D.B.). A.M. acknowledges support by the Dolce & Gabbana fashion company. M.L. was the recipient of a fellowship from AIRC (code 25307).

Conflict of Interest statement: The authors have declared that no conflict of interest exist.

References

1. Zhu N, et al. A Novel Coronavirus from Patients with Pneumonia in China, 2019. *N. Engl. J. Med.* 2020;382(8):727–733.

2. Guan W, et al. Clinical Characteristics of Coronavirus Disease 2019 in China. *N. Engl. J. Med.* 2020;382(18):1708–1720.

3. Liu F, et al. Prognostic value of interleukin-6, C-reactive protein, and procalcitonin in patients with COVID-19. *J. Clin. Virol. Off. Publ. Pan Am. Soc. Clin. Virol.* 2020;127:104370.

4. Merad M, Martin JC. Pathological inflammation in patients with COVID-19: a key role for monocytes and macrophages. *Nat. Rev. Immunol.* 2020;20(6):355–362.

5. Zhang Q, et al. Inborn errors of type I IFN immunity in patients with life-threatening COVID-19. *Science* 2020;370(6515):eabd4570.

6. Bastard P, et al. Autoantibodies against type I IFNs in patients with life-threatening COVID-19. *Science* 2020;370(6515):eabd4585.

7. Cabeza-Cabrerizo M, et al. Dendritic Cells Revisited. *Annu. Rev. Immunol.* [published online ahead of print: January 22, 2021]; doi:10.1146/annurev-immunol-061020-053707

8. Sozzani S. Dendritic cell trafficking: More than just chemokines. *Cytokine Growth Factor Rev.* 2005;16(6):581–592.

9. Villadangos JA, Schnorrer P. Intrinsic and cooperative antigen-presenting functions of dendritic-cell subsets in vivo. *Nat. Rev. Immunol.* 2007;7(7):543–555.

10. Asselin-Paturel C, et al. Type I interferon dependence of plasmacytoid dendritic cell activation and migration. *J. Exp. Med.* 2005;201(7):1157–1167.

11. Blanco P, et al. Dendritic cells and cytokines in human inflammatory and autoimmune diseases. *Cytokine Growth Factor Rev.* 2008;19(1):41–52.

514 12. Swiecki M, Colonna M. The multifaceted biology of plasmacytoid dendritic cells. *Nat. Rev. Immunol.*
515 2015;15(8):471–485.

516 13. Uematsu S, Akira S. Toll-like Receptors and Type I Interferons. *J. Biol. Chem.* 2007;282(21):15319–
517 15323.

518 14. Jarrossay D, et al. Specialization and complementarity in microbial molecule recognition by human
519 myeloid and plasmacytoid dendritic cells. *Eur. J. Immunol.* 2001;31(11):3388–3393.

520 15. Shimizu T. Structural insights into ligand recognition and regulation of nucleic acid-sensing Toll-like
521 receptors. *Curr. Opin. Struct. Biol.* 2017;47:52–59.

522 16. Cervantes JL, et al. TLR8: the forgotten relative revindicated. *Cell. Mol. Immunol.* 2012;9(6):434–438.

523 17. Zhou R, et al. Acute SARS-CoV-2 Infection Impairs Dendritic Cell and T Cell Responses. *Immunity*
524 2020;53(4):864-877.e5.

525 18. Peruzzi B, et al. Quantitative and qualitative alterations of circulating myeloid cells and plasmacytoid DC
526 in SARS-CoV-2 infection. *Immunology* 2020;161(4):345–353.

527 19. Sozzani S, et al. Trafficking properties of plasmacytoid dendritic cells in health and disease. *Trends*
528 *Immunol.* 2010;31(7):270–277.

529 20. Heil F. Species-Specific Recognition of Single-Stranded RNA via Toll-like Receptor 7 and 8. *Science*
530 2004;303(5663):1526–1529.

531 21. Salvi V, et al. Exosome-delivered microRNAs promote IFN-α secretion by human plasmacytoid DCs via
532 TLR7. *JCI Insight* 2018;3(10). doi:10.1172/jci.insight.98204

533 22. Diebold SS, et al. Nucleic acid agonists for Toll-like receptor 7 are defined by the presence of uridine
534 ribonucleotides. *Eur. J. Immunol.* 2006;36(12):3256–3267.

535 23. Salvi V, et al. TLR Signalling Pathways Diverge in Their Ability to Induce PGE2. *Mediators Inflamm.*
536 2016;2016:5678046.

24. Hornung V, et al. Quantitative Expression of Toll-Like Receptor 1–10 mRNA in Cellular Subsets of Human Peripheral Blood Mononuclear Cells and Sensitivity to CpG Oligodeoxynucleotides. *J. Immunol.* 2002;168(9):4531–4537.

25. Muzio M, et al. Differential expression and regulation of toll-like receptors (TLR) in human leukocytes: selective expression of TLR3 in dendritic cells. *J. Immunol. Baltim. Md 1950* 2000;164(11):5998–6004.

26. Zhang S, et al. Small-molecule inhibition of TLR8 through stabilization of its resting state. *Nat. Chem. Biol.* 2018;14(1):58–64.

27. Kužnik A, et al. Mechanism of Endosomal TLR Inhibition by Antimalarial Drugs and Imidazoquinolines. *J. Immunol.* 2011;186(8):4794–4804.

28. Fabbri M, et al. MicroRNAs bind to Toll-like receptors to induce prometastatic inflammatory response. *Proc. Natl. Acad. Sci.* 2012;109(31):E2110–E2116.

29. Li Y, et al. Extraordinary GU-rich single-strand RNA identified from SARS coronavirus contributes an excessive innate immune response. *Microbes Infect.* 2013;15(2):88–95.

30. Moreno-Eutimio MA, López-Macías C, Pastelin-Palacios R. Bioinformatic analysis and identification of single-stranded RNA sequences recognized by TLR7/8 in the SARS-CoV-2, SARS-CoV, and MERS-CoV genomes. *Microbes Infect.* 2020;22(4–5):226–229.

31. Scheuplein VA, et al. High secretion of interferons by human plasmacytoid dendritic cells upon recognition of Middle East respiratory syndrome coronavirus. *J. Virol.* 2015;89(7):3859–3869.

32. Cervantes-Barragán L, et al. Type I IFN-Mediated Protection of Macrophages and Dendritic Cells Secures Control of Murine Coronavirus Infection. *J. Immunol.* 2009;182(2):1099–1106.

33. Dyavar SR, et al. Role of toll-like receptor 7/8 pathways in regulation of interferon response and inflammatory mediators during SARS-CoV2 infection and potential therapeutic options. *Biomed. Pharmacother.* 2021;141:111794.

34. van der Made CI, et al. Presence of Genetic Variants Among Young Men With Severe COVID-19. *JAMA* [published online ahead of print: July 24, 2020]; doi:10.1001/jama.2020.13719

35. Onodi F, et al. SARS-CoV-2 induces human plasmacytoid pre-dendritic cell diversification via UNC93B and IRAK4. *BioRxiv Prepr. Serv. Biol.* [published online ahead of print: January 8, 2021]; doi:10.1101/2020.07.10.197343

36. Kouwaki T, et al. Extracellular Vesicles Deliver Host and Virus RNA and Regulate Innate Immune Response. *Int. J. Mol. Sci.* 2017;18(3):666.

37. Campbell GR, et al. Human Immunodeficiency Virus Type 1 Nef Inhibits Autophagy through Transcription Factor EB Sequestration. *PLOS Pathog.* 2015;11(6):e1005018.

38. Wang K, et al. CD147-spike protein is a novel route for SARS-CoV-2 infection to host cells. *Signal Transduct. Target. Ther.* 2020;5(1):283.

39. Collin M, Bigley V. Human dendritic cell subsets: an update. *Immunology* 2018;154(1):3–20.

40. Sharma NK, et al. Is a COVID-19 vaccine developed by nature already at work?. *Med. Hypotheses* 2020;145:110335.

41. Borges RC, Hohmann MS, Borghi SM. Dendritic cells in COVID-19 immunopathogenesis: insights for a possible role in determining disease outcome. *Int. Rev. Immunol.* 2020;1–18.

42. Zhang Q, et al. Life-Threatening COVID-19: Defective Interferons Unleash Excessive Inflammation. *Med N. Y. N* 2020;1(1):14–20.

43. Chow KT, Gale M, Loo Y-M. RIG-I and Other RNA Sensors in Antiviral Immunity. *Annu. Rev. Immunol.* 2018;36(1):667–694.

44. Viswanathan T, et al. Structural basis of RNA cap modification by SARS-CoV-2. *Nat. Commun.* 2020;11(1):3718.

45. Toldo S, et al. Inflammasome formation in the lungs of patients with fatal COVID-19. *Inflamm. Res.* [published online ahead of print: October 20, 2020]; doi:10.1007/s00011-020-01413-2

584 46. Rodrigues TS, et al. Inflammasomes are activated in response to SARS-CoV-2 infection and are
585 associated with COVID-19 severity in patients. *J. Exp. Med.* 2021;218(3). doi:10.1084/jem.20201707

586 47. Xiao TS. The nucleic acid-sensing inflammasomes. *Immunol. Rev.* 2015;265(1):103–111.

587 48. Becker CE, O'Neill LAJ. Inflammasomes in inflammatory disorders: the role of TLRs and their
588 interactions with NLRs. *Semin. Immunopathol.* 2007;29(3):239–248.

589 49. Campbell GR, et al. SARS-CoV-2, SARS-CoV-1, and HIV-1 derived ssRNA sequences activate the
590 NLRP3 inflammasome in human macrophages through a non-classical pathway. *iScience* 2021;24(4):102295.

591 50. Marass F, Upton C. Sequence Searcher: A Java tool to perform regular expression and fuzzy searches of
592 multiple DNA and protein sequences. *BMC Res. Notes* 2009;2:14.

593 51. Salvi V, et al. Dual regulation of osteopontin production by TLR stimulation in dendritic cells. *J. Leukoc.*
594 *Biol.* 2013;94(1):147–158.

595 52. Cossarizza A, et al. Guidelines for the use of flow cytometry and cell sorting in immunological studies
596 (second edition). *Eur. J. Immunol.* 2019;49(10):1457–1973.

597 53. Del Prete A, et al. The Atypical Receptor CCRL2 Is Essential for Lung Cancer Immune Surveillance.
598 *Cancer Immunol. Res.* 2019;7(11):1775–1788.

599

600

601

602

603

604

605

606

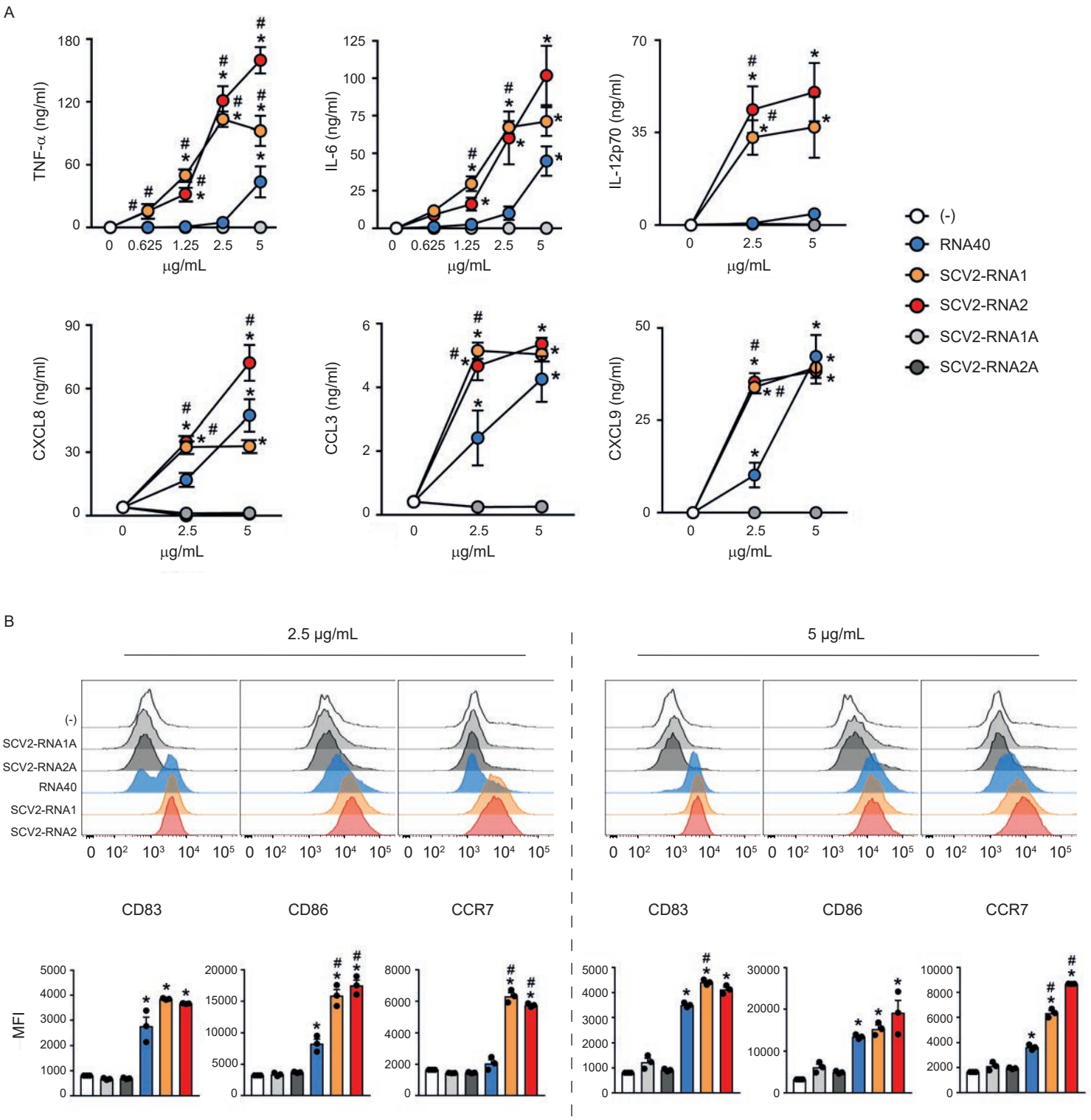

Figure 1. SAMPs activate cytokine secretion and phenotypical maturation of moDCs. (A) moDCs ($2x10^6$/ml) were stimulated with increasing concentrations of the indicated viral RNAs or with vehicle alone (-) for 24 hours. The production of TNF-α, IL-6, IL-12p70, CXCL8, CCL3 and CXCL9 was evaluated by ELISA in cell-free supernatants. Data are expressed as mean ± SEM (n=3). Results of SCV2-RNA1A and SCV2-RNA2A are superimposed in all graphs. (B) moDCs were stimulated as described in (A) and the surface expression of CD83, CD86 and CCR7 evaluated by FACS analysis. Data are expressed as representative cytofluorimetric profiles (upper panels) or as the mean ± SEM (n=3) of the Median of Fluorescence Intensity (MFI) (lower panels). (A-B) *P< 0.05 versus (-) by one-way ANOVA with Dunnett's post-hoc test; #P< 0.05 versus RNA40 by paired Student's *t* test.

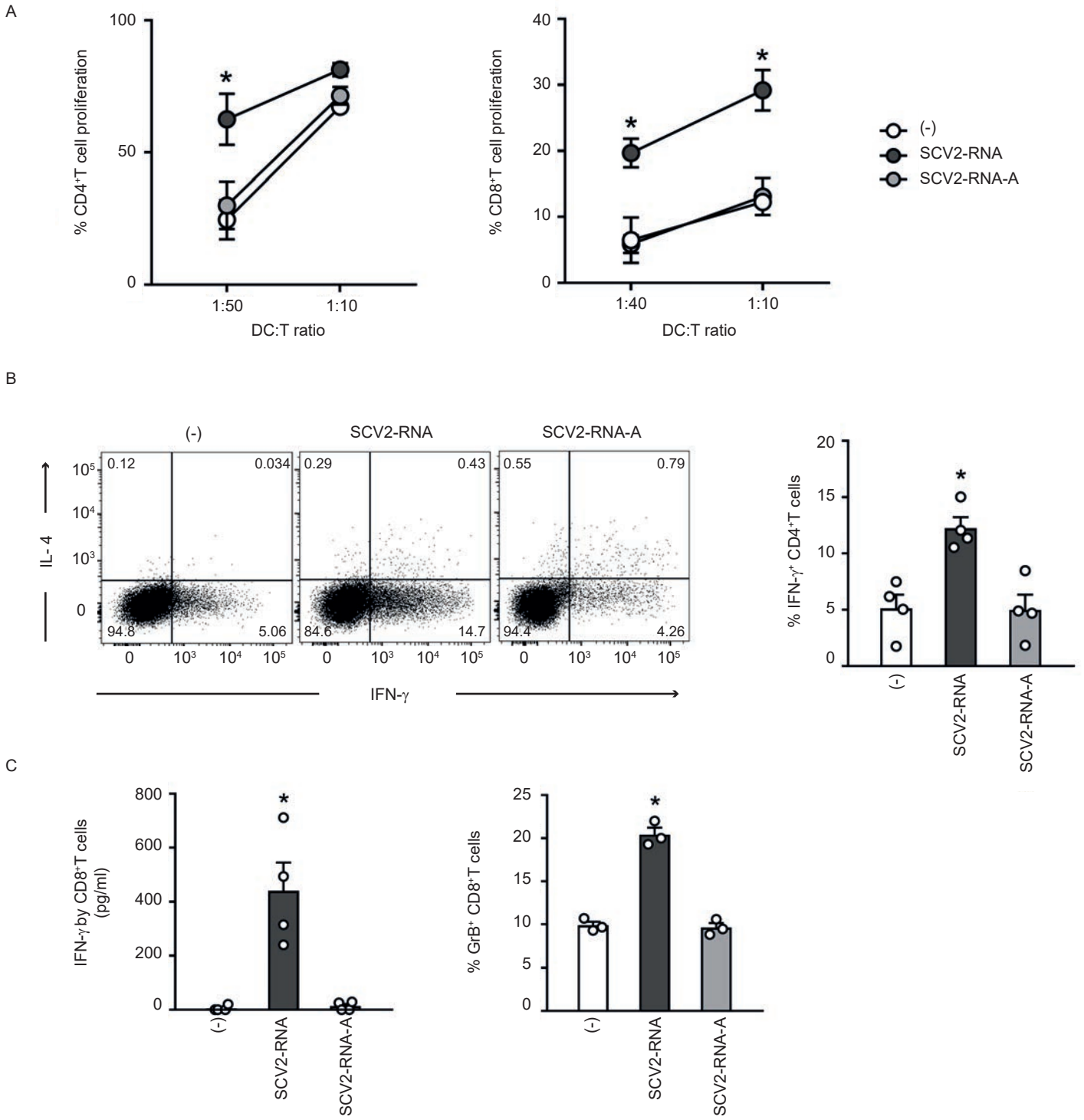

Figure 2. SAMP-activated DCs trigger T cell proliferation and functional activation. (A) moDCs were stimulated with vehicle (-) or with SCV2-RNA or the A-to-U-replaced SCV2-RNA-A (both at 5 μg/ml) for 24 hours. Activated moDCs were co-cultured for 6 days with CFSE-stained allogenic naïve $CD4^+$ T cells or $CD8^+$ T cells at the indicated DC:T cell ratio. Alloreactive T cell proliferation was assessed by measuring CellTrace-CFSE dye loss by flow cytometry. Data are expressed as mean ± SEM (n=3) of the percentage of proliferating T cells. (B) moDCs stimulated as in (A) were cocultured for 6 days with allogenic naïve $CD4^+$ T (DC:T cell ratio 1:20). Intracellular IFN-γ and IL-4 were evaluated by FACS analysis. Left, dot plots from one representative experiment out of four is shown. Right, bar graphs from four independent experiments. Data are expressed as mean ± SEM of the percentage of IFN-γ-producing cells. (C) moDCs activated as in (A) were cocultured for 6 days with allogenic $CD8^+$ T (DC:T cell ratio 1:10). IFN-γ production was evaluated by ELISA in cell-free supernatants and intracellular Granzyme B (GrB) by FACS analysis. Data are expressed as mean ± SEM (n=3). (A-C) *P< 0.05 versus (-) by one-way ANOVA with Dunnett's post-hoc test.

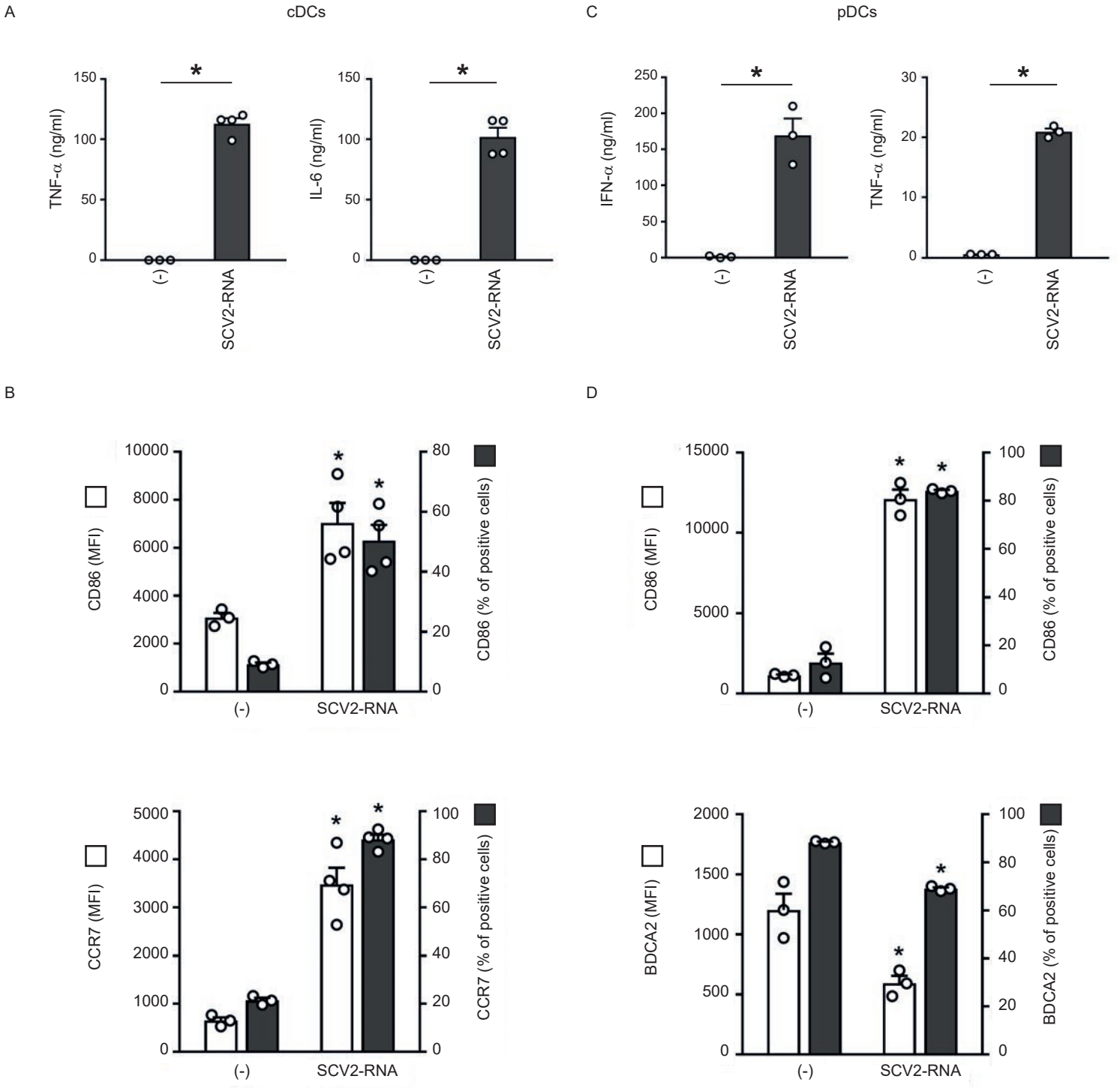

Figure 3. SAMPs activate cytokine secretion and phenotypical maturation in primary circulating DC subsets. cDCs (2x10^6/ml) and pDCs (1x10^6/ml) were stimulated with 5 μg/ml SCV2-RNA for 24 hours. (A-C) Cytokine secretion was evaluated by ELISA. Data are expressed as mean ± SEM (n=3-4); *P< 0.05 versus (-) by paired Student's *t* test. (B-D) Surface expression of CD86, CCR7 and BDCA2 was evaluated by FACS analysis. Data are expressed as mean ± SEM of the median fluorescence intensity (MFI) (left y axis), as well as the mean ± SEM of the percentage of positive cells (right y axis) (n=3-4); *P< 0.05 versus (-) by paired Student's *t* test.

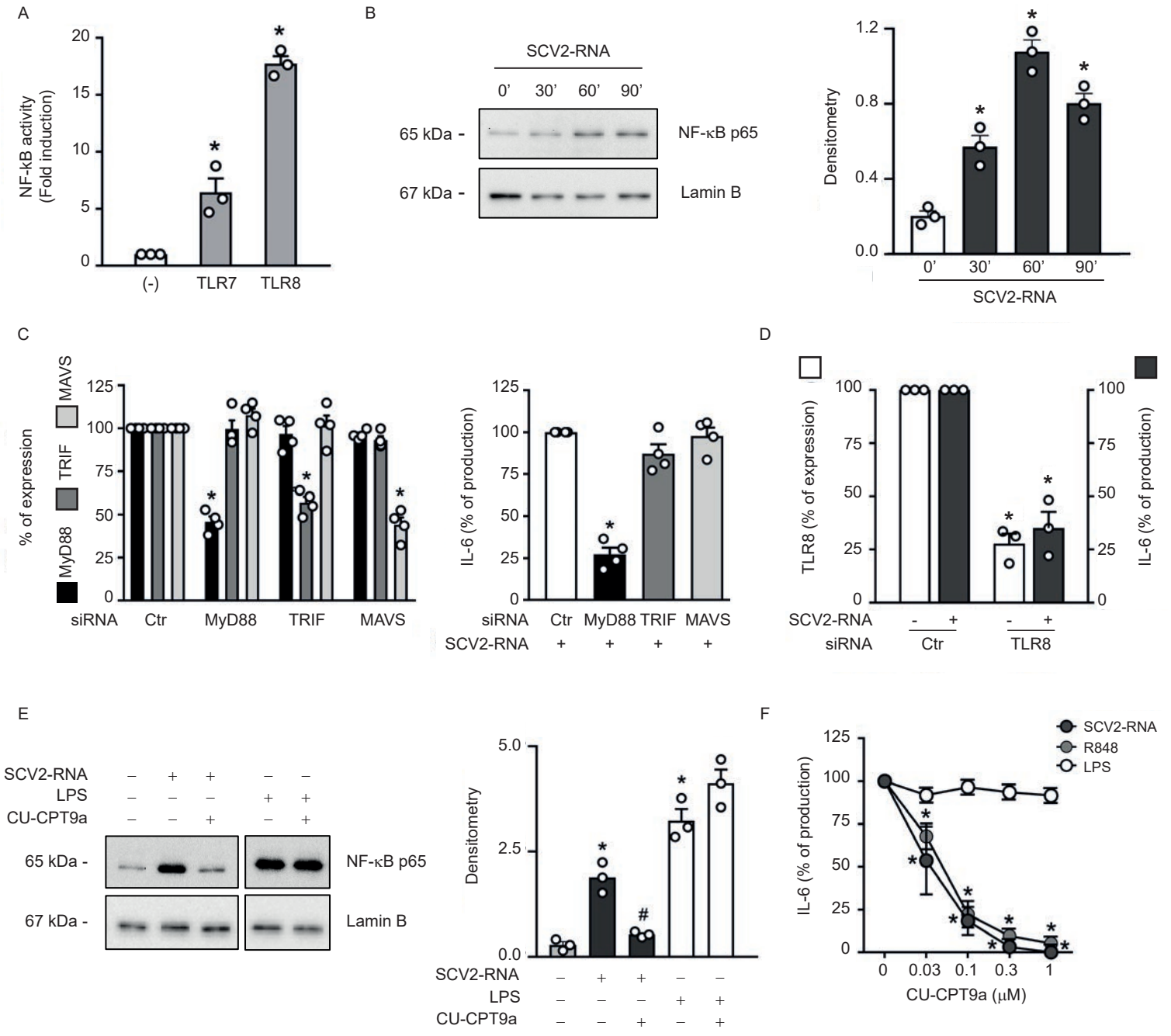

Figure 4. SAMPs activate the TLR8/MyD88/NF-κB axis in moDCs. (A) HEK-293 cells stably transfected with human TLR7, TLR8 or luciferase alone (-) were stimulated with SCV2-RNA for 24 hours. NF-κB activation was evaluated as luciferase activity. Data are expressed ad mean ± SEM (n=3); *P< 0.05 versus (-) by one-way ANOVA with Dunnett's post-hoc test. (B-E) moDCs were stimulated with SCV2-RNA as indicated (B) or pre-treated with CU-CPT9a (1 μM) and then stimulated with SCV2-RNA or LPS for 1 hour (E). Nuclear extracts were blotted against NF-κB p65 and Lamin B. One representative donor and densitometry of three donors are shown. *P< 0.05 versus untreated by one-way ANOVA with Dunnett's post-hoc test; #P< 0.05 versus "SCV2-RNA" by paired Student's *t* test. (C, left panel) moDCs were transfected with indicated siRNAs and target gene expression evaluated by qPCR. Results depict percentage of target gene expression (mean ± SEM n=4). (C, right panel) moDCs transfected with indicated siRNAs were stimulated with SCV2-RNA for 24 hours and IL-6 production evaluated by ELISA. Data are expressed as percentage of production (n=4); *P< 0.05 versus "ctr siRNA" by one-way ANOVA with Dunnett's post-hoc test. (D) moDCs were transfected with indicated siRNAs and the expression of TLR8 was evaluated by qPCR (left y axis, white bars). IL-6 production upon SCV2-RNA stimulation was evaluated by ELISA (right y axis, grey bars). Data (percentage of expression/production) represent the mean ± SEM (n=3); *P< 0.05 versus respective "ctr" by paired Student's *t* test. (F) moDCs were pre-treated with CU-CPT9a, then stimulated as indicated for 24 hours and IL-6 production evaluated by ELISA. Data are expressed as percentage of production for each individual stimulation (n=3); *P< 0.05 versus respective "0" by one-way ANOVA with Dunnett's post-hoc test.

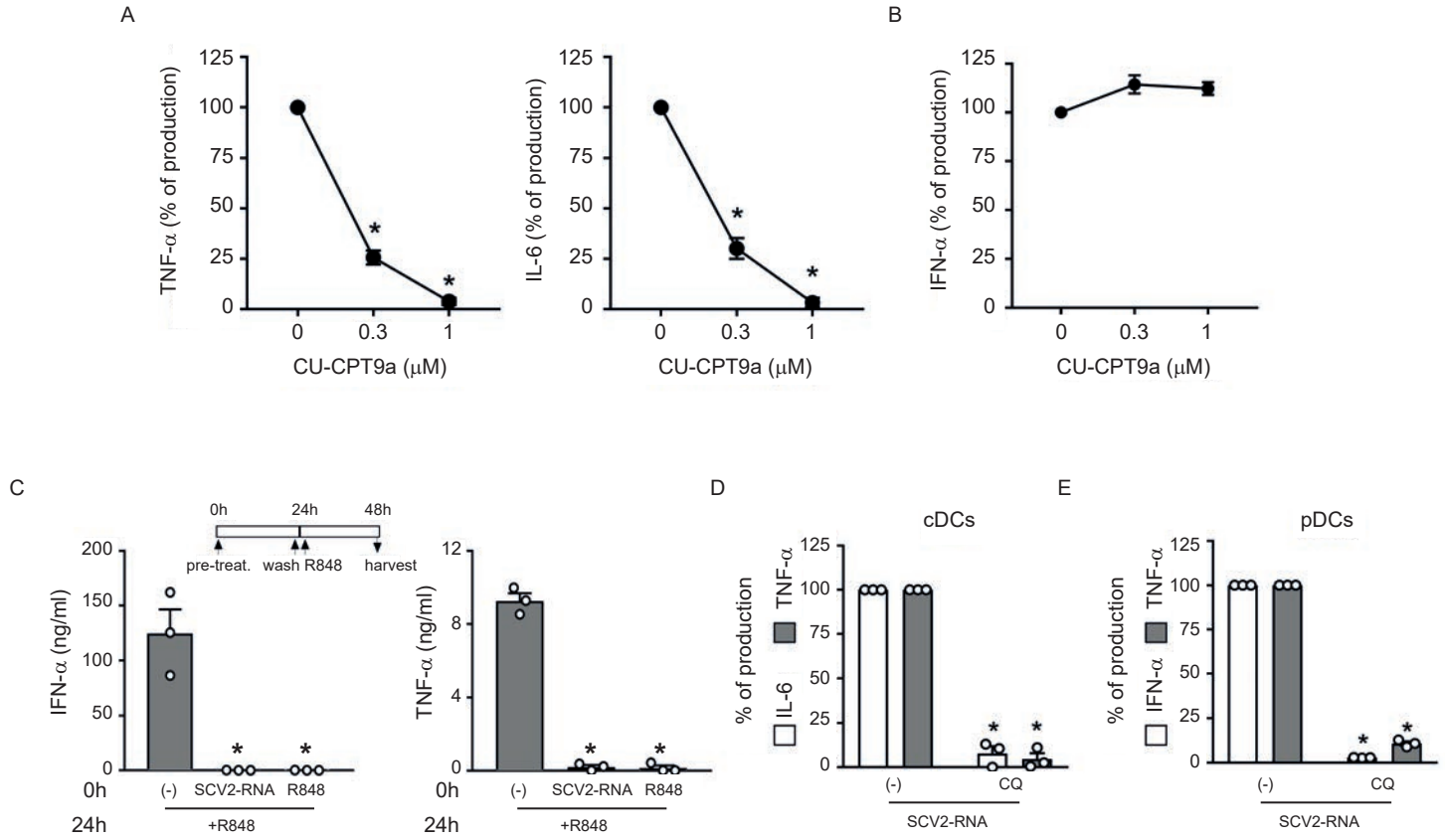

Figure 5. TLR7 and TLR8 are responsible for primary DC activation by SAMPs. cDCs (A) and pDCs (B) were pre-treated with increasing concentration of CU-CPT9a and then stimulated with SCV2-RNA (5 μg/ml) for 24 hours. Secreted TNF-α, IL-6 and IFN-α were quantified by ELISA. Data are expressed as percentage of production (n=3); *P< 0.05 versus "0" by one-way ANOVA with Dunnett's post-hoc test. (C) pDCs were pre-treated (0h) with SCV2-RNA (5 μg/ml) or R848 (1 μg/ml) or left untreated for 24 hours, washed and restimulated with R848 for additional 24 hours. Secreted IFN-α and TNF-α were quantified by ELISA. Data are expressed as mean ± SEM (n=3); *P< 0.05 versus "(-)" by one-way ANOVA with Dunnett's post-hoc test. (D) cDCs were pre-treated for 1 hour with Chloroquine (CQ, 10 μM) and then stimulated with SCV2-RNA (5 μg/ml) for 24 hours. Secreted IL-6 (white bars) and TNF-α (grey bars) were evaluated by ELISA. Data are expressed as percentage of production (n=3); *P< 0.05 versus respective "(-) SCV2-RNA" by paired Student's *t* test. (E) pDCs were pre-treated for 1 hour with CQ (10 μM) and then stimulated with SCV2-RNA (5 μg/ml) for 24 hours. Secreted IFN-α (white bars) and TNF-α (grey bars) were quantified by ELISA. Data are expressed as percentage of production (n=3); *P< 0.05 versus respective "(-) SCV2-RNA" by paired Student's *t* test.

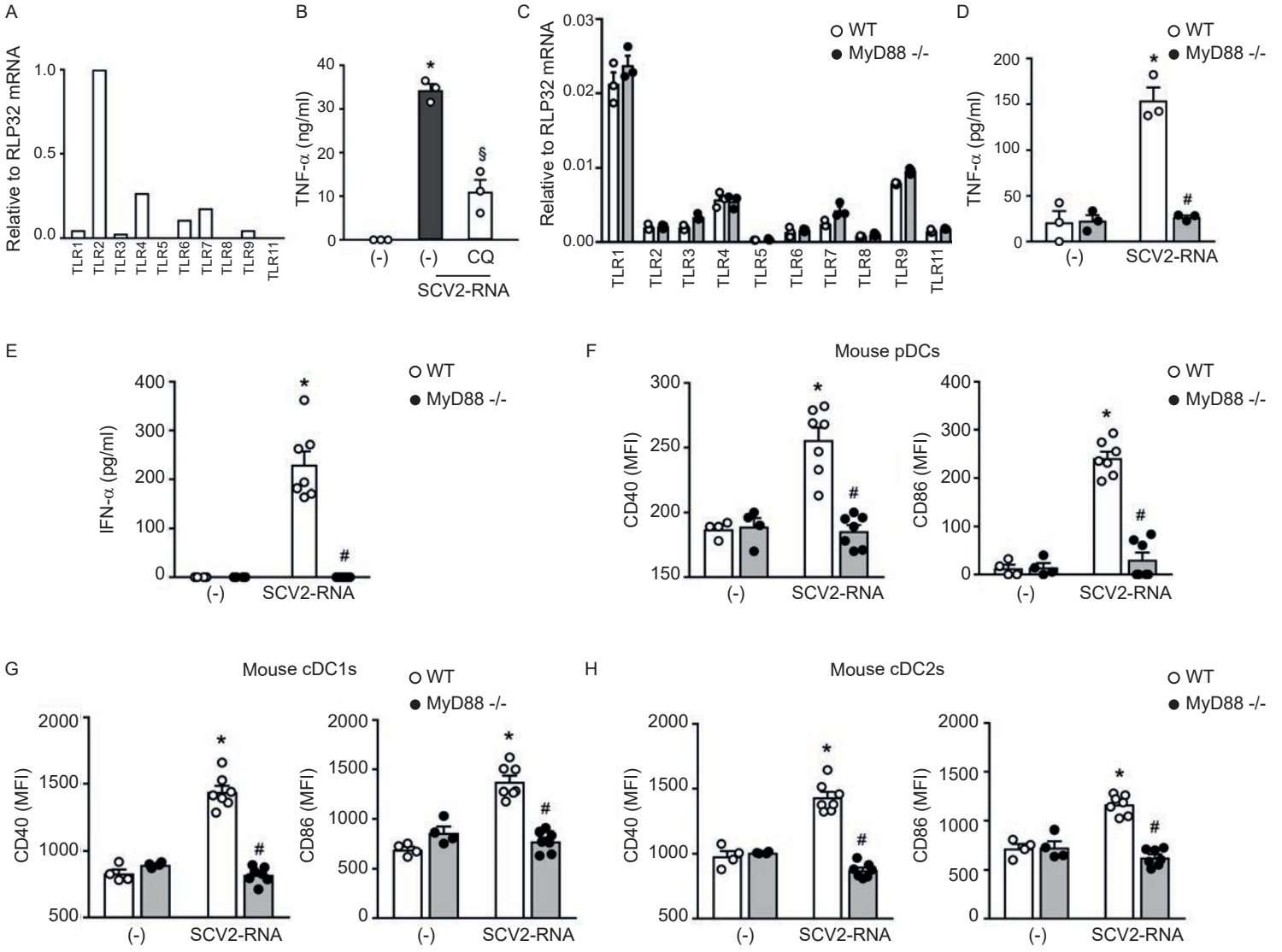

Figure 6. SAMPs activate murine cells *in vitro* and *in vivo*. (A) Expression of *TLR* mRNAs in RAW264.7 cells. Data are expressed as $2^{-\Delta Ct}$ relative to RPL32 of one representative experiment out of three. (B) RAW264.7 ($1x10^6$/ml) were pre-treated for 1 hour with CQ (12.5 μM), then stimulated with 5 μg/ml SCV2-RNA or vehicle (-) for 24 hours. Secreted TNF-α was evaluated by ELISA. Data are expressed as mean ± SEM (n=3); *P< 0.05 versus (-); §P<0.05 versus "(-) SCV2-RNA" by paired Student's *t* test. (C) Expression of TLR mRNAs in splenocytes from WT (white circle) or MyD88$^{-/-}$ mice (black circle). Data are expressed as mean ± SEM (n=3) of $2^{-\Delta Ct}$ relative to RPL32 of one representative experiment out of three. (D) Splenocytes ($3x10^6$/ml) from WT (white circle) or MyD88$^{-/-}$ mice (black circle) were stimulated with 5 μg/ml SCV2-RNA or vehicle (-) for 24 hours. Secreted TNF-α was evaluated by ELISA. Data are expressed as mean ± SEM (n=3); *P< 0.05 versus (-) or #P < 0.05 versus "SCV2-RNA MyD88$^{-/-}$" by paired Student's *t* test. (E) Circulating IFN-α in WT (white circle) or MyD88$^{-/-}$ mice (black circle) treated with SCV2-RNA or vehicle (-) for 6 hours. Data are expressed as mean ± SEM ((-) n=4, SCV2-RNA n=7); *P< 0.05 versus (-) or #P < 0.05 versus "SCV2-RNA MyD88$^{-/-}$" by unpaired Student's *t* test of one representative experiment out of three. (F-H) Activation of splenic pDCs (CD11c^{int}MHC-II$^+$B220$^+$SiglecH$^+$) (F), cDC1s (CD11c$^+$MHC-II$^+$CD8α$^+$CD11b$^-$) (G) or cDC2s (CD11c$^+$MHC-II$^+$CD8α$^-$CD11b$^+$) (H) from WT (white circle) or MyD88$^{-/-}$ mice (black circle), treated with SCV2-RNA or vehicle (-) for 6 hours evaluated in terms of CD40 and CD86 expression. Data are expressed as mean ± SEM of the median fluorescence intensity (MFI) ((-) n=4, SCV2-RNA n=7); *P< 0.05 versus (-) or #P < 0.05 versus "SCV2-RNA MyD88$^{-/-}$" by unpaired Student's *t* test.

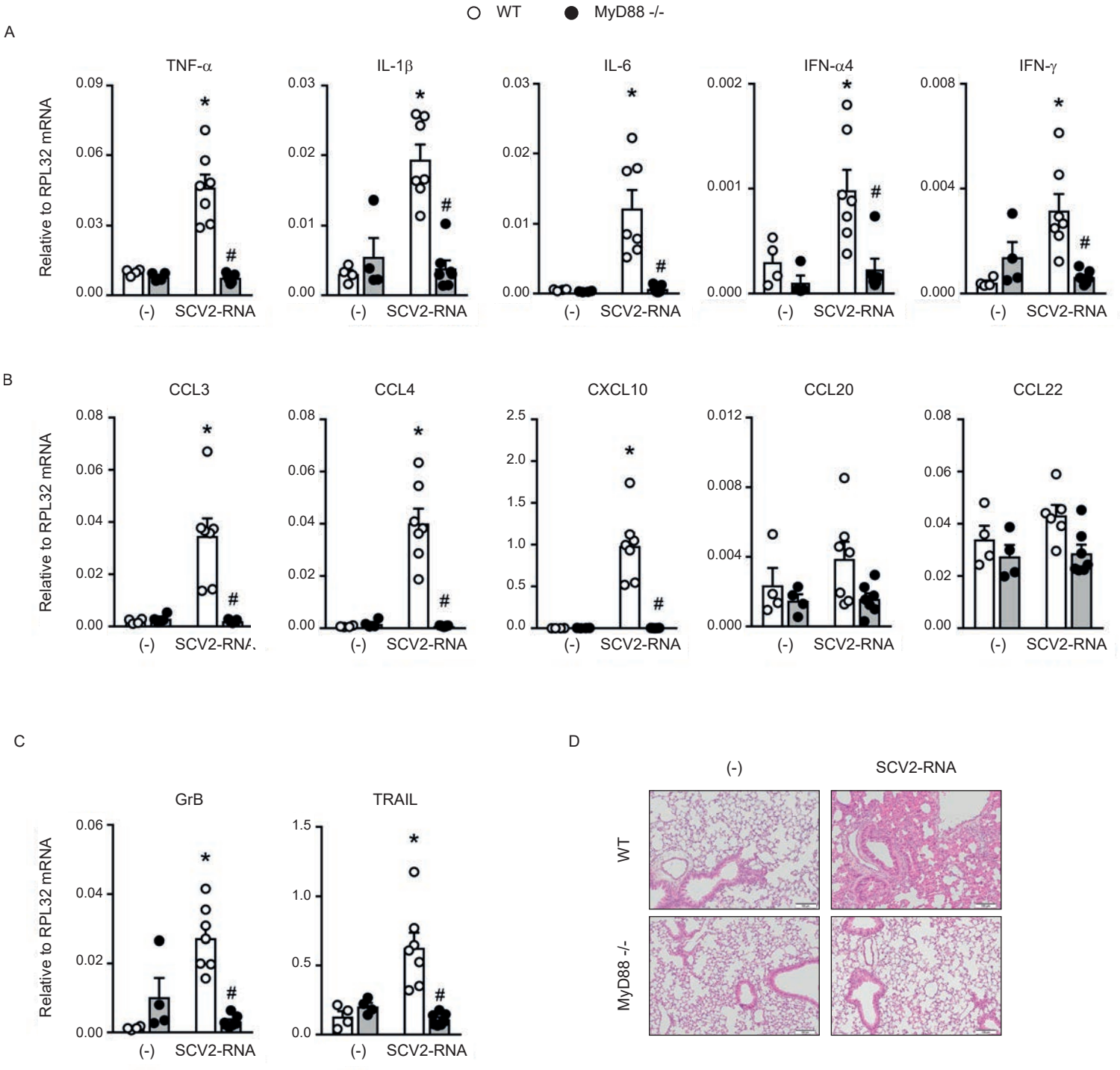

Figure 7. SAMPs induce inflammation *in vivo*. (A-C) Real-time PCR for cytokines, chemokines and effector proteins in lungs of WT (white circle) or MyD88$^{-/-}$ (black circle) treated or not with SCV2-RNA for 6 hours. Data are expressed as mean ± SEM ((-) n=4, SCV2-RNA n=7) of $2^{-\Delta Ct}$ relative to housekeeping mRNA (*RPL32*); *P< 0.05 versus (-) or $^{\#}$P < 0.05 versus "SCV2-RNA MyD88$^{-/-}$" by unpaired Student's *t* test of one representative experiment out of three. (D) Histological evaluation of lungs from WT or MyD88$^{-/-}$ mice treated or not with SCV2-RNA for 6 hours. Image shows one section out of the three longitudinal serial sections performed of one representative left lung out of 7. Scale bars = 100 μm.